Optical Engineering

SPIEDigitalLibrary.org/oe

Effect of structural recession on the performance of a satellite laser retroreflector

Hui Zhou
Song Li

SPIE

Effect of structural recession on the performance of a satellite laser retroreflector

Hui Zhou
Song Li
Wuhan University
School of Electronic Information
Wuhan 430079, China
E-mail: abidingmyself@163.com

Abstract. Satellite laser retroreflector (LRR) array is an essential reflecting element for satellite laser ranging. Because of the requirements of manufacturing and assembling, the actual LRR reflecting face is placed underneath the top of assembly. We use the ray tracing method to build up the active retroreflecting region model for LRR with a structural recession effect. Combined with the principle of far-field diffraction intensity and velocity aberration, we give the mathematical model for expressing the structural recession effect on the received optical signal intensity (ROSI) by a ground station. As an important factor for determining the performance of LRR, the distribution of ROSI is simulated for an HY-2A LRR array. The simulation shows that the value of ROSI decreases along with the increment of structural recession size. The bigger optical incident angle should bring about further reduction of ROSI. Only considering the structural recession effect on ROSI, we obtain the regularity of difference of range correction. Before and after considering the structural recession effect, the maximum difference of range correction reaches 9.36 mm for the whole incidence condition. It demonstrates that structural recession cannot be ignored for deciding the performance of LRR. [DOI: 10.1117/1.OE.52.4.043001]

Subject terms: laser retroreflector; structural recession effect; ray tracing; active retroreflecting region; received optical signal intensity.

Paper 130021 received Jan. 6, 2013; revised manuscript received Mar. 22, 2013; accepted for publication Mar. 25, 2013; published online Apr. 16, 2013.

1 Introduction

Satellite laser retroreflector (LRR) is a solid tetrahedron composed of three mutually perpendicular reflecting surfaces and one front face, which is the indispensable component in satellite laser ranging to reflect the laser beams directly back to the ground station.[1] For the purpose of preventing it from being damaged during handling, LRR is usually manufactured with mounting tabs to hold it conveniently into the protective housing.[2–4] However, due to the protection manners, practical solid retroreflector designs require mounting structures that result in their reflecting surfaces being recessed with respect to their front window faces. With the structural recession effect, the active retroreflecting region (ARR) of LRR is diminished for the oblique incidence of laser beams. Considering the performance of LRR, including the received optical signal intensity (ROSI), is subject to the ARR, the analysis of structural recession effect on ROSI becomes more important.

In the past, the effect of structural recession on ARR has been expounded qualitatively.[5] Evidently, investigating the relationship between structural recession size and the LRR performance quantitatively is not enough. In this paper, we apply a ray tracing method to calculate the ARR. The influence of structural recession on the mathematical model of ROSI is then described. Combined with the parameters of an HY-2A satellite LRR, the direct and indirect effects of structural recession on ROSI and range correction of LRR array are studied by computer simulation.

2 Active Retroreflecting Region Model

The ARR is an aperture on the front face of LRR, which is established by restricting the positions of a ray on the LRR surface.

The schematic of the LRR mounting assembly is illustrated in Fig. 1. The LRR is held by a ring assembly within a cylindrical shield. The upper and lower mounting rings fit over tabs to encircle the LRR. A retainer ring or encloser (RoE) on the top of upper mounting rings presses the LRR assembly against a structural frame. Taking into consideration that the reflecting faces of LRR lie on the bottom of the upper mounting rings, the LRR can be treated as structural recession. Figure 1 shows that the structural recession parameters include the distance d_2 from the top of the tab to the front face of LRR, and the distance d_1 from the front face of the LRR to the RoE.

The reflecting face coordinate system (RCS) (x, y, z) used to describe the geometry of the LRR is shown in Fig. 2. For a better indication of each direction of incident ray, we define the front face coordinate system (FCS) (x', y', z'), where the z' axis is the symmetry of the LRR, and y' axis is the projection of the y-axis upon the front face.

The coordinate system transformation relationship between RCS and FCS can be expressed by Ref. 6

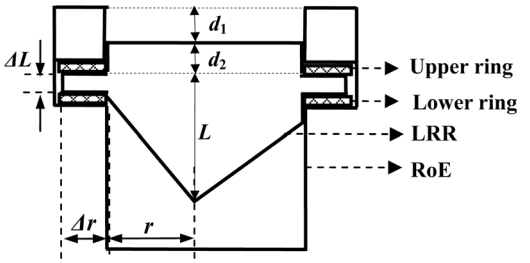

Fig. 1 Schematic of laser retroreflector (LRR) mounting assembly; RoE = retainer ring or encloser.

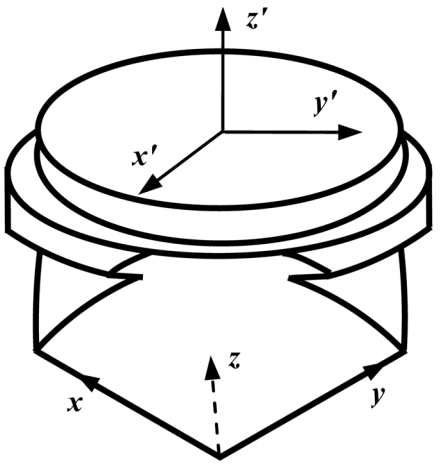

Fig. 2 Definition of coordinate system for the reflecting face coordinate system (RCS) and front face coordinate system (FCS).

$$\begin{bmatrix} x \\ y \\ z \end{bmatrix} = M \begin{bmatrix} x' \\ y' \\ z' \end{bmatrix} + N = \begin{pmatrix} \frac{\sqrt{2}}{2} & -\frac{\sqrt{6}}{6} & \frac{\sqrt{3}}{3} \\ 0 & \frac{\sqrt{6}}{3} & \frac{\sqrt{3}}{3} \\ -\frac{\sqrt{2}}{2} & -\frac{\sqrt{6}}{6} & \frac{\sqrt{3}}{3} \end{pmatrix} \begin{bmatrix} x' \\ y' \\ z' \end{bmatrix} + \begin{bmatrix} \frac{L+d_1+d_2}{\sqrt{3}} \\ \frac{L+d_1+d_2}{\sqrt{3}} \\ \frac{L+d_1+d_2}{\sqrt{3}} \end{bmatrix}, \quad (1)$$

where M is the transformation matrix, and L is the vertex length of the LRR in Fig. 1.

If the incident ray with the incident angle φ and the azimuth angle θ is incident on the LRR, the direction cosine R_0 of the incident ray in the FCS is written by

$$R_0 = (R_{0x}, R_{0y}, R_{0z}) = (\sin\varphi\cos\theta, \sin\varphi\sin\theta, \cos\varphi). \quad (2)$$

Then, the incident ray vector can be rewritten as $R = MR_0$ in the RCS. The incident ray undergoes two refractions at the front face and three reflections at the reflecting face. The position and direction at each face can be traced by a ray tracing approach. There are six different orders of reflections determined by where the ray strikes the LRR.

We consider the case in which the incident ray is refracted by the front face and reflected successively by the $y-z$, $x-z$, and $x-y$ planes, then refracted again by the front face. According to the vector form of the refraction, if we ignore the effect of the LRR manufacture error on the direction of ray, we can obtain the direction cosine of the refracted and reflected ray in the RCS as

$$\begin{aligned} &Rr = (\alpha, \beta, \gamma) = nR + \sqrt{1 - n^2\sin^2\varphi} - n\cos\varphi, \\ &Rx = (-\alpha, \beta, \gamma), Ry = (-\alpha, -\beta, \gamma), Rz = (-\alpha, -\beta, -\gamma), \end{aligned} \quad (3)$$

where n is the refractive index of the LRR material.

Because the active reflecting region is represented in the FCS, we assume that the coordinate of the incidence point is $(x_1', y_1', 0)$. For ease of calculation, we get another coordinate from using Eq. (1) with (x_1, y_1, z_1). Therefore, we can calculate the positions $(0, y_2, z_2)$, $(x_3, 0, z_3)$, $(x_4, y_4, 0$, and (x_5, y_5, z_5) on the LRR surface by using the direction cosines, incident point coordinates of the ray, and equations for the LRR surface. To give a better restrictive description of the leaving point (x_5, y_5, z_5), we convert its coordinate from the RCS to FCS, and it can be expressed as $(x_5', y_5'0)$.

The positions on the front face should be distributed within the circular front face, except for the incident and outgoing rays that passed through them cannot intersect with the RoE. The positions on the reflecting face must be located within the active reflection region, which is the same distribution form for the three reflecting faces. In terms of a schematic of the LRR, Fig. 3 illustrates the region boundary condition (RBC) for the positions on the front face and x–y reflecting face.

Based on the RBC for the positions with the abovementioned reflections order, we can express the first ARR as

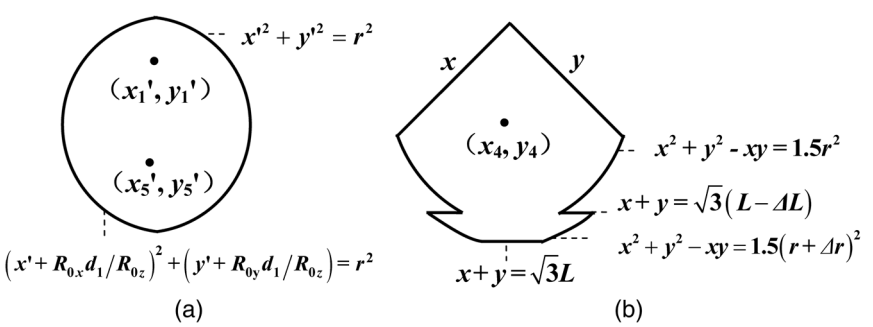

Fig. 3 Region boundary condition for the positions on laser retroreflector (LRR) surface: (a) front face; (b) x-y reflecting face. The parameter r is the radius of the front face, and Δr and ΔL are the width and height, respectively, of tabs in Fig. 1.

$$Q_1 = \{(x_1', y_1') \in B_f \quad \text{and} \quad (x_5', y_5') \in B_f \quad \text{and} \quad (x_4, y_4) \in B_{xy} \quad \text{and} \quad (y_2, z_2) \in B_{yz} \quad \text{and} \quad (x_3, z_3) \in B_{xz}\}, \tag{4}$$

where B_f, B_{xy}, B_{yz}, and B_{xz} indicate the regions surrounded by the front face, $x-y$ plane, y–z-plane, and x–z-plane RBC, respectively.

We can calculate the other five ARRs in the same manner for the remaining orders of reflections, which can be denoted as Qj $(j = 2, 3, \ldots, 6)$.

3 Effect of Structural Recession on the Performance of a Satellite Laser Retroreflector

In a satellite laser ranging system, LRR is used to retroreflect a laser beam transmitted by a ground station, and support the ground station to implement the satellite laser ranging.[7] The performance of satellite LRR can be regarded as the ROSI zby the ground station. A schematic of the system can be described in Fig. 4.

Due to the relative velocity between the satellite and ground station, the reflected laser beam shifts with the slightest angle aberration, which can be given approximately as[8]

$$\Delta\varphi = \frac{2}{c}\sqrt{\frac{R_e^2 g}{R_e + h}}\cos\varphi. \tag{5}$$

Here, R_e is the Earth radius, $g = 9.8\ \mathrm{m/s^2}$ is the gravitational acceleration at the surface, h is the satellite height above sea level, and c is the velocity of light. The plane coordinate of the velocity aberration position is written as $(h\Delta\varphi, 0)$.

Given that the distance between the LRR and ground station is far greater than the ARR, the ROSI is treated as far-field diffraction intensity (FFDI) at the velocity aberration position. According to Kirchhoff's diffraction equation, we can solve the ROSI approximately by the following expression:

$$I(\varphi,\theta,d_1,d_2) = \left|\frac{1}{\lambda i}\sum_{j=1}^{6}\iint_{Qj}\frac{U_t}{\rho}\exp\{i[(2\pi/\lambda)\rho + W]\}\mathrm{d}x'\mathrm{d}y'\right|^2, \tag{6}$$

where the amplitude U_t of the field on the LRR front face is assumed to be homogeneous; λ is the wavelength of the incident laser beam; ρ is the distance between points on the LRR front face and velocity aberration position; W is the phase of the reflected beam from the LRR, which has a relationship with the dihedral angle offset and flatness error.[9]

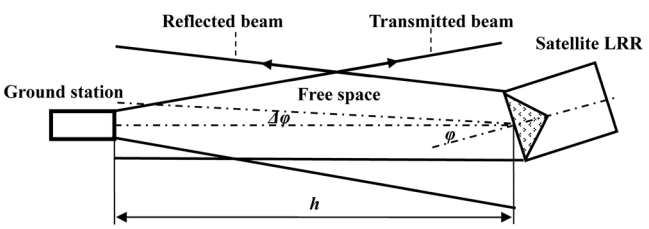

Fig. 4 Working principle schematics of a satellite laser ranging system with a laser retroreflector (LRR).

The ROSI is a function of the optical incidence condition and LRR structural recession size in the case that other parameters of LRR are known. To expatiate the effect of structural recession, we introduce a new factor η, which represents the decrease in the ROSI due to d_1 and d_2. On the basis of Eq. (6), η can be described as

$$\eta(\varphi,\theta,d_1,d_2) = \frac{I(\varphi,\theta,d_1,d_2)}{I(\varphi,\theta,0,0)}. \tag{7}$$

The attenuation coefficient η is determined by the optical incidence condition (φ,θ) and structural recession sizes, which falls in the range of 0–1.

4 Simulation for the Effect of Structural Recession on the ROSI

The HY-2A satellite is a marine remote sensing satellite developed by China, which is equipped with the LRR array as a cooperative target for satellite laser ranging.[10] The HY-2A satellite LRR array consists of nine LRRs, which are equally mounted on a regular 48-deg pyramid frame with one nadir-looking LRR in the center. The structure of the HY-2A satellite LRR array is shown in Fig. 5.

Each LRR is made from fused quartz glass, whose reflecting faces are silver-coated. Except for structural recession sizes, other parameters of the LRR are indicated in Table 1, which are the initial conditions for calculating the ROSI.

According to the parameters of the LRR and ARR model, the distributions of the ARR with different LRR structural recession sizes and an optical incidence condition (30 deg, 0 deg) are illustrated in Fig. 6. The d/L ratio is applied to generalize the calculation results for all values of L.

Figure 6 shows that ARRs are composed of six sections that correspond with six orders of reflections, which are indicated as six colors. The shape of all ARRs approaches an ellipse. With the increment of structural recession sizes, the dimension of ARRs diminishes gradually. The reduction effect of the structural recession parameter d_1 on the ARRs is evidently much stronger than structural recession parameter d_2.

Considering that the ARRs vary with the appearance of structural recession, the attenuation coefficient η associated with the ROSI will present a corresponding change. The simulation in Fig. 7 shows the distribution regularities of η with

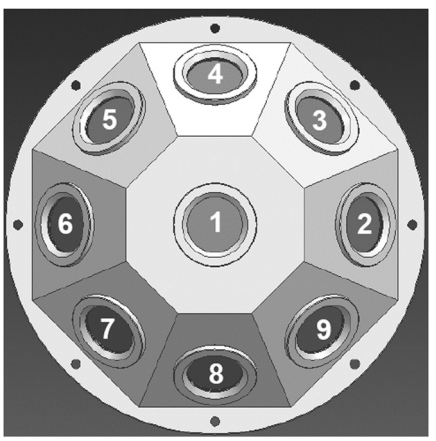

Fig. 5 Diagram of HY-2A satellite laser retroreflector (LRR) array.

Table 1 Parameters of the HY-2A satellite laser retroreflector.

Radius of the front face (mm)	16.5
Vertex length (mm)	23.3
Tabs height (mm)	5
Tabs width (mm)	2
Dihedral angle offset (arcsec)	1.6”
Surface flatness	$\lambda/10$ ($\lambda = 632.8$ nm)
Index of refraction	1.461

different structural recession sizes for three optical incidence conditions (10 deg, 0 deg), (20 deg, 0 deg), and (30 deg, 0 deg).

We observe that η falls off rapidly due to the augment of structural recession size for the above three incidence conditions. For any given structural recession size, the value of η falls more quickly with an increasing incident angle. By comparing two groups of η distribution curves in Fig. 7(a) and 7(b), we have obtained that structural recession size d_1 has a stronger effect on the fall-off extent of η when compared to structural recession size d_2 at the same incident angle.

The comprehensive effect of structural recession parameters d_1 and d_2 on the attenuation coefficient η with an incidence condition (20 deg, 0 deg) is simulated in Fig. 8. The

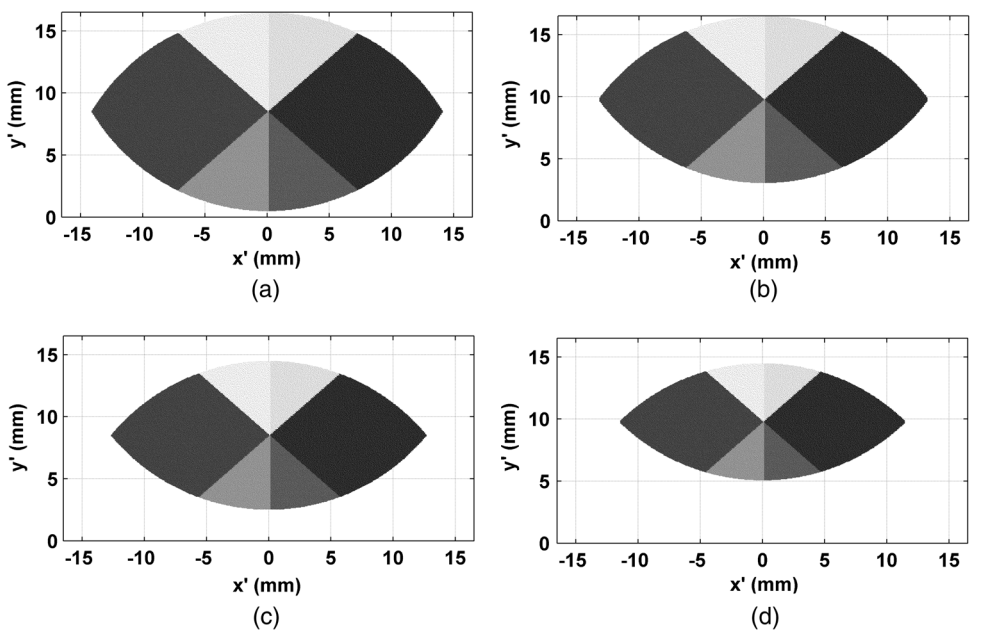

Fig. 6 Distributions of active retroreflecting regions (ARRs) with different laser retroreflector (LRR) structural recession sizes for $\varphi = 30$ deg, $\theta = 0$ deg: (a) $d_1/L = 0$ $d_2/L = 0$; (b) $d_1/L = 0$, $d_2/L = 0.15$; (c) $d_1/L = 0.15$, $d_2/L = 0$; (d) $d_1/L = 0.15$, $d_2/L = 0.15$.

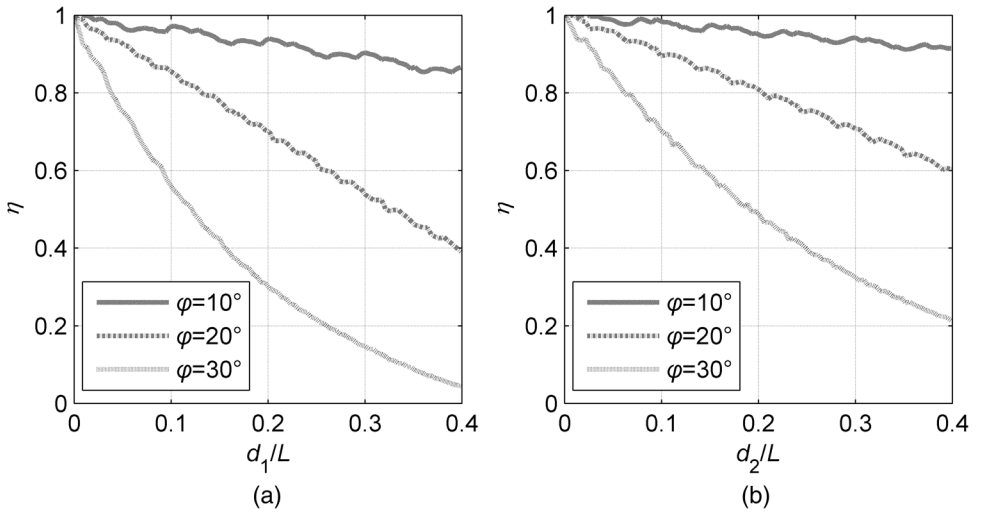

Fig. 7 Distribution of η with different structural recession sizes for three optical incidence conditions (10 deg, 0 deg), (20 deg, 0 deg), and (30 deg, 0 deg): (a) d_1/L; (b) d_2/L.

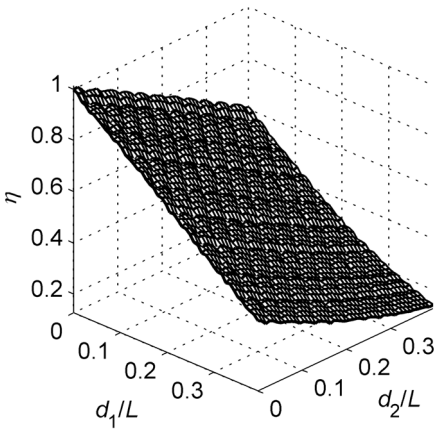

Fig. 8 Distribution of η due to the comprehensive effect of structural recession parameter d_1 and d_2 for the incidence condition (20 deg, 0 deg).

distribution of η can be described approximately as slanted plane. The slope in the d_1 direction is obviously bigger than the d_2 direction, which validates again, that the influence degree of d_1 on η is greater than d_2. For the purpose of better assembling the HY-2A LRR, the structural recession sizes of d_1 and d_2 are chosen as 2.5 and 2.8 mm, respectively. We get the relationship curve between incident angle and attenuation coefficient η in Fig. 9. The attenuation coefficient η decreases rapidly with an increasing incident angle. The value of η is almost equal to zero as a result of the restriction of structural recession effect when incident angle is 40 deg. The range correction is the distance of the centroid of ROSI from the center of the satellite LRR array, which can be given by Ref. 11

$$S(\phi,\Theta,d_1,d_2)=\frac{\sum_{m=1}^{\text{num}} S_m I(\varphi_m,\theta_m,d_1,d_2)}{\sum_{m=1}^{\text{num}} I(\varphi_m,\theta_m,d_1,d_2)}, \tag{8}$$

where Φ and Θ are incident angle and azimuth angle, respectively, in the LRR array coordinate. The relationship between them and the incidence condition (φ_m,θ_m) of individual LRRs can be converted by the structural matrix of LRR array; num is the number of LRRs in LRR array; S_m is

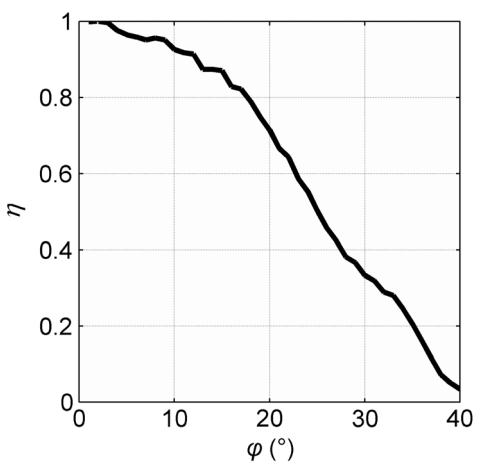

Fig. 9 Relationship curve between the incident angle and η for the HY-2A laser retroreflector (LRR).

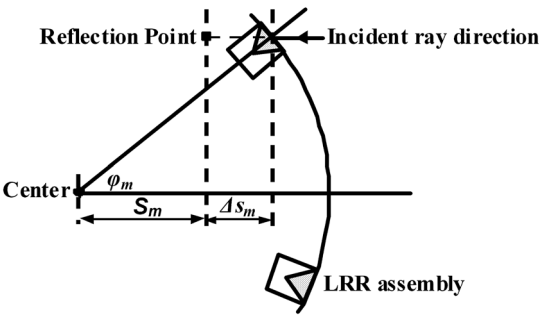

Fig. 10 Diagram of definition for the location of reflection point for m'th laser retroreflector (LRR).

the distance of the apparent reflection point for the m'th LRR from the plane through the center of satellite LRR array perpendicular to the incident ray. The definition of S_m is indicated in Fig. 10.

The symbol ΔS_m represents the distance between the incidence point and reflection point for m'th LRR.[12] According to the definition of the distance S_m, it can be calculated by using a general model:[13]

$$S_m = b_m \cos\varphi_m - L\sqrt{n^2-\sin^2\varphi_m}, \tag{9}$$

where b_m is the distance of the LRR front faces from the center of LRR array.

Considering the variety of the ROSI by the structural recession effect, the range correction of the LRR array will present a few undulations. In the general case, if we ignore the structural recession effect on S_m, we may use the following expression to indicate the differences of range correction as

$$\Delta e(\phi,\Theta,d_1,d_2)=S(\phi,\Theta,0,0)-S(\phi,\Theta,d_1,d_2). \tag{10}$$

In terms of Eq. (10) and the HY-2A LRR array parameters, Fig. 11 shows the contour distribution of the difference of range correction. In Fig. 11, the numbers around the circumference and radial direction represent the values of Θ and Φ.

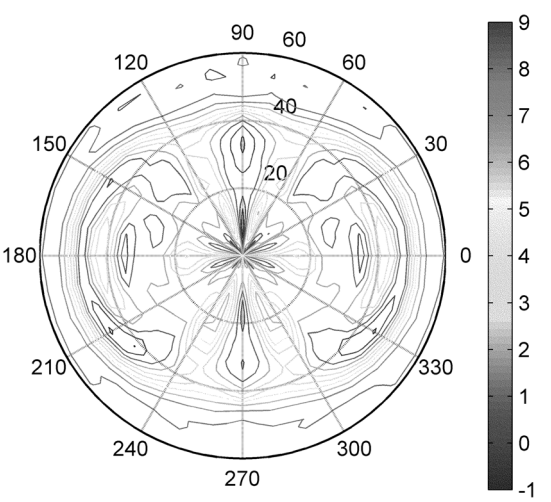

Fig. 11 Contour distribution of the difference of range corrections for incidence conditions.

The contour distribution of the differences of range correction is irregular with the change of Θ and Φ. The differences of range correction are confined between -1.81 and 9.36 mm. As for satellite laser ranging with millimeter accuracy, the differences cannot be neglected. It demonstrates the importance of analyzing the structural recession effect on the ROSI.

5 Conclusion

We use the ray tracing method and FFDI theory of an LRR to investigate the structural recession effect on the performance of an LRR array. The simulations on the ARR and ROSI demonstrate that structural recession parameters have strong effects on them, which result in reducing the ARR and ROSI with the increment of structural recession size. The extent of reduction depends on the optical incidence condition. A greater incident angle should bring about further reduction of the ROSI. On the basis of the analysis results, we obtain the difference of range correction when the structural recession effect on the ROSI is considered for the HY-2A satellite LRR array. The results show that the structural recession effect cannot be neglected when calculating the range correction for an LRR array.

References

1. D. Currie, S. D. Agnelloc, and G. D. Monache, "A lunar laser ranging retroreflector array for the 21st century," *Acta Astronaut.* **68**(7–8), 667–680 (2011).
2. S. Dell'Agnello et al., "Creation of the new industry-standard space test of laser retroreflectors for the GNSS and LAGEOS," *Adv. Space Res.* **47**(5), 822–842 (2011).
3. A. Paolozzi, I. Ciufolini, and C. Vendittozzi, "Engineering and scientific aspects of LARES satellite," *Acta Astronaut.* **69**(3–4), 127–134 (2011).
4. S. Dell'Agnello et al., "SCF-Test of a Galileo-IOV retroreflector and thermal-optical simulation of a novel GNSS retroreflector array on a critical orbit," in *Proc. IEEE 1st AESS European Conf. on Satellite Telecommunications*, pp. 1–6, IEEE, Rome (2012).
5. D. A. Arnold, "Method of calculating retroreflector-array transfer functions," SAO Special Report #382 (1979).
6. S. Li, B. Tang, and H. Zhou, "Calculation on diffraction aperture of cube corner retroreflector," *Chin. Opt. Lett.* **6**(11), 833–836 (2008).
7. R. Nair and K. W. Goossen, "Effect of face separation in corner-cube reflectors," *Opt. Eng.* **48**(12), 123003 (2009).
8. J. J. Degnan, "Millimeter accuracy satellites for two color ranging," in *Proc. Int. Workshop Las. Ranging Instrument.*, Vol. 7, pp. 36–51, National Aeronautics and Space Administration, Annapolis, Maryland (1992).
9. H. Zhou, S. Li, and G. Zheng, "The phase mode of reflected beam from laser retroreflector with dihedral angle and flatness error," *Opt. Rev.* **18**(1), 1–6 (2011).
10. B. Wu, M. Lin, and Z. Zhang, "Global SLR tracking support for HY-2 satellite precise orbit determination," in *Proc. Int. Workshop Las. Ranging Instrument.*, Vol. 48, pp. 382–384, Verlag des Bundesamtes für Kartographie und Geodasie, Bad Koetzting, Germany (2011).
11. N. T. Mironov et al., "ETALON-1, -2 center of mass correction and array reflectivity," in *Proc. Int. Workshop Las. Ranging Instrument.*, Vol. 6, pp. 9–32, National Aeronautics and Space Administration, Annapolis, Maryland (1992).
12. M. W. Fitzmaurice et al., "Prelaunch testing of the laser geodynamic satellite (LAGEOS)," NASA Tech. Paper 1062 (1977).
13. T. Otsubo, J. Amagai, and H. Kunimori, "The center of mass correction of the geodetic satellite AJISAI for single-photon laser ranging," *IEEE Trans. Geosci. Rem. Sens.* **37**(4), 2011–2018 (1999).

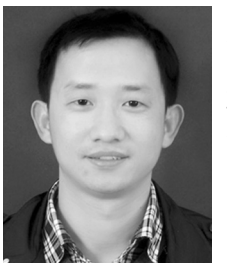

Hui Zhou received his BE in mechanical engineering in 2001, and his PhD in laser remote sensing in 2007 from Wuhan University, China. His current research focuses on the signal process for a satellite laser altimeter and design for a satellite LRR array.

Song Li received her BE in 1986 and ME in 1989 in optical engineering from Wuhan Technical University of Surveying and Mapping, China, and her PhD in surveying engineering in 2002 from Wuhan University, China. Her current research focuses on photoelectric detection, laser interferometry, and laser atmospheric detection.